Journal of Intelligent Systems and Control
https://www.acadlore.com/journals/JISC

Phase Shift Modulation Control of Single Stage Dual Active Bridge AC to DC Converter in Overmodulation Region

Maha F. Ahmed, Mohamad N. Abdul Kadir*

Department of Electrical Engineering, University of Mosul, 41002 Mosul, Iraq

* Correspondence: Mohamad N. Abdul Kadir (makadr@uomosul.edu.iq)

Received: 01-20-2025 **Revised:** 02-24-2025 **Accepted:** 03-12-2025

Citation: M. F. Ahmed and M. N. Abdul Kadir, "Phase shift modulation control of single stage dual active bridge AC to DC converter in overmodulation region," *J. Intell Syst. Control*, vol. 4, no. 2, pp. 10–20, 2025. https://doi.org/10.56578/jisc040102.

Abstract: Efficient bidirectional energy exchange between an alternating current (AC) grid and a direct current (DC) source has been enabled through advanced power converter topologies. In this study, a single-stage AC-DC dual active bridge (DAB) converter employing phase-shift modulation (PSM) was investigated, with a particular focus on performance within the overmodulation regime. Bidirectional switching modules were implemented on the AC side to facilitate seamless energy transfer. Two conventional modulation strategies—sinusoidal and triangular—and a novel back-calculated modulation method were examined for their performance in both linear and overmodulation operating regions. The proposed back-calculation method incorporates an off-line generated reference current waveform designed to approximate linear control characteristics while substantially minimizing current harmonic distortion under overmodulated conditions. This approach extends the linear relationship between the reference current and power transfer capability beyond the conventional modulation limits, thereby enhancing converter performance in high-demand scenarios. Simulation-based analysis demonstrated that, in the linear region, the proposed method reduced average current total harmonic distortion (THD) by at least 45% when compared to conventional sinusoidal and triangular modulation techniques. Moreover, within the overmodulation regime, the linear correlation between the reference current and power transfer was extended by approximately 16.5%. The current harmonic distortion remained below 5% and 8% at modulation ratios of 108% and 112%, respectively, underscoring the robustness of the proposed strategy. These results suggest that the proposed PSM method is highly effective in achieving improved power exchange with reduced harmonic content in both linear and overmodulated operation, thereby offering a viable solution for high-performance AC-DC power conversion in smart grids and renewable energy systems.

Keywords: AC-DC converter; Bidirectional converter; Dual active bridge; Overmodulation; Phase-shift modulation

1 Introduction

The power generated by the photovoltaic (PV) system follows a bell-shaped pattern throughout the day, with the highest power output available for approximately one hour [1]. Additionally, significant fluctuations in peak solar power across seasons have been observed [2]. Consequently, designing the power converter to handle the maximum peak power while operating in linear mode leads to underutilization of components. This study aims to investigate the PSM-controlled converter's operation in the overmodulation mode, enabling higher power harvesting during the occasional peak intervals.

The most prevalent configuration for PV inverter systems is the DAB converter [3]. The basic converter design consists of two stages: the AC-DC stage and the DC-DC stage. The AC-DC stage is commonly implemented using either an uncontrolled rectifier, which supplies a fixed-voltage DC link [4], or an active front-end rectifier that maintains a regulated DC link voltage while enabling independent control of the power factor [5, 6]. Although this two-stage configuration provides the advantage of decoupled active and reactive power control, recent investigations have explored alternative single-stage AC-DC topologies to achieve improved system compactness and reduced component count [5, 7–9]. In alignment with these emerging approaches, the present work adopts a more integrated

single-stage design, thereby contributing to the development of more compact and efficient PV power conversion systems.

The configuration presented by Baranwal et al. [7] demonstrates a single-stage AC-DC conversion setup achieved through a push-pull conversion stage. This stage incorporates a center-tapped primary winding along with bidirectional switching modules. The design is based on a half-bridge AC converter with gallium nitride (GaN) devices and a full-bridge DC converter. Chen et al. [8] adopted a single-stage DAB topology. To mitigate voltage overshoot, a snubber capacitor was integrated to establish a pathway for current stemming from the leakage inductance.

The single-stage AC-DC DAB system described by Llomplat et al. [9] encompasses a two-winding transformer alongside a full-bridge converter located at the AC side. The AC bridge was implemented using bidirectional switches. The PSM strategy was used in DC-DC DAB converters to control the power flow between the primary and secondary sides. In PSM-controlled converters, the phase-shift angle (δ) determines the magnitude and direction of the transferred power. The advantages of PSM include high power conversion efficiency, high power density and bidirectional power transfer [10, 11].

In a PSM AC-DC DAB converter, power flow changes periodically over the AC line voltage cycle. To track a reference sinusoidal current, the phase-shift angle changes throughout the AC period. If the slowly changing AC voltage and the reference current are considered constant within the switching cycle, PSM control with periodically changing phase-shift angle can be employed. The modulation function defines the variation of the phase-shift angle during the AC cycle [9].

Several innovative designs of a single-stage isolated bidirectional AC-DC converter have been proposed by researchers. A novel approach combines a three-phase DAB converter with a nine-switch matrix converter to achieve both high efficiency and compactness. This topology combines the benefits of the DAB converter's high efficiency and the matrix converter's compact design. By introducing synchronous pulse width modulation (PWM) control, the switching frequency of the matrix converter can be reduced by 44%, leading to efficiency enhancement of the tested 1 kW system [12]. Chen et al. [13] optimized the matrix-based converter for power density and cost and achieved a high power factor. However, the smaller capacitance introduces noticeable capacitor voltage ripples during switching cycles, which can compromise zero-voltage-switching (ZVS) operation and increase electromagnetic interference (EMI) [13].

To address the non-linear power control limitations of traditional PSM, Guo et al. [14] proposed a variable frequency PSM technique. This strategy combines frequency modulation with an extended phase shift (EPS) method to simplify the controller algorithm. The approach enables the use of a high-frequency filter capacitor at the output DC link, replacing bulky electrolytic capacitors and enhancing system safety and power density. Simulation results validate the effectiveness of this control strategy in achieving efficient energy conversion. To enhance power conversion efficiency in variable frequency PSM-controlled DAB converters, Komeda et al. [15] considered an active energy buffer. The control approach adjusts the switching frequency based on the phase angle of the single-phase AC-line voltage, enabling continuous-current-mode (CCM) operation. The variable frequency operation approach, however, complicates the control and the magnetic core permeability degrades at higher frequencies.

To reduce harmonic distortion of a single-stage DAB that is used to link a PV system to the grid, Ahmed and AbdulKadir [16] derived a modified modulation function. This back calculation modulation function (BCMF) determines the phase-shift angle as a function of the instantaneous reference current. With the same technique, any current waveform within the maximum limit can be tracked using this method.

The aim of this study is to enhance the power transfer capability of the same converter presented by Ahmed and AbdulKadir [16] by transferring higher fundamental current between the AC and DC sides. It is known that the maximum current transfer in a DC-DC converter is achieved at a phase-shift angle of $\pi/2$ [5–7]. In AC-DC converters, this limit determines the maximum peak AC current [16]. The suggested approach is based on the extension of the concept of overmodulation. In this study, the term overmodulation denotes the scenario where the control signal exceeds the value corresponding to the maximum current limit $(\pi/2)$. The overmodulation mode in conventional PWM-controlled converters leads to higher power flow, but it is accompanied by nonlinear control and higher distortion. Consequently, it can be anticipated that the overmodulation region in PSM allows higher power flow, which can be considered for managing the occasional peak output power of the PV system. This study also presents a novel approach to address the side effects of higher distortion and non-linearity.

This study is organized as follows: Section 2 presents the single-stage AC-DC DAB converter, including the switching states and the AC-side current equation. Section 3 defines the two traditional modulation functions in the linear and overmodulation regions. Section 4 describes the BCMF and its extension to the overmodulation region. This is followed by the simulation and results in Section 5. Finally, the conclusions are presented in Section 6.

2 Single-stage AC-DC Converter and Switching States

The single-phase, single-stage AC-DC power converter, as shown in Figure 1, was used to link a DC source to a single-phase AC grid. The voltage of the single-phase AC grid is given by:

$$V_{ac}(t) = V_{ac,p} \sin(\omega_o t) \tag{1}$$

where, $V_{ac,p}$ is the peak of the AC voltage. In addition, $\omega_o = 2\pi f_o$, where f_o is the grid frequency (Hz). As shown in Figure 1, the AC side converter is a full bridge converter that uses bidirectional switching modules, formed by two Metal-Oxide-Semiconductor Field-Effect Transistors (MOSFETs), denoted by S_{XA} and S_{XB}, to withstand the bipolar AC voltage. The reversible power flow management and isolation are achieved through the high-frequency transformer and the auxiliary series inductor, denoted by L_a. The DC H-bridge switches are denoted by Q_1 and Q_2. The switching states and the resultant voltages are defined in Table 1.

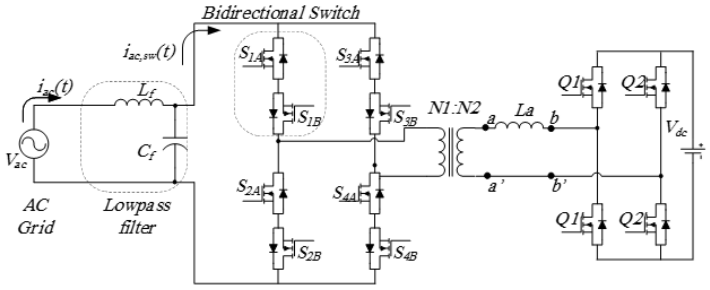

Figure 1. Single-phase single-stage AC-DC power converter

Table 1. Switching states and the corresponding voltages

Vac	S_{1A}, S_{4A}	S_{1B}, S_{4B}	S_{2A}, S_{3A}	S_{2B}, S_{3B}	$Q1$	$Q2$	V_{La}
>0	1	1	0	1	1	0	$nv_{ac} - V_{dc}$
>0	1	1	0	1	0	1	$nv_{ac} + V_{dc}$
>0	0	1	1	1	1	0	$-nv_{ac} - V_{dc}$
>0	0	1	1	1	0	1	$-nv_{ac} + V_{dc}$
<0	1	1	1	0	1	0	$nv_{ac} - V_{dc}$
<0	1	1	1	0	0	1	$nv_{ac} + V_{dc}$
<0	1	0	1	1	1	0	$-nv_{ac} - V_{dc}$
<0	1	0	1	1	0	1	$-nv_{ac} + V_{dc}$

The voltage between the terminals of b and b' is imposed by the DC H-bridge. While the AC H-bridge imposes the voltage between terminals a and a', the basic PSM concept is to regulate power transmission by adjusting the phase shift between the modulated voltages v_{aa} and v_{bb}. The inductor voltage ($v_{La} = v_{aa'} - v_{bb'}$) determines the power flow between the AC and DC sides [16]. The operation of the DAB converter is illustrated in Figure 2, showing the transition of electrical energy between the AC and DC sides. In subgraph (a) of Figure 2, the situation is depicted when the AC voltage is in the positive half cycle. During this phase, all MOSFETs, designated as B (SxB), are conducting, allowing the converter to operate as a full-bridge converter via the four switches (S1A-S4A). Subgraph (b) of Figure 2 illustrates the condition when the AC voltage is within the negative half cycle. In this instance, all MOSFETs, designated as A (SxA), are activated, enabling the converter to function as a full-bridge converter through the four switches (S1B-S4B). As electrical energy transfers from the AC side over to the DC side, Figure 2 illustrates both the AC converter and the converters on the DC side voltages. The voltage across the inductor La is the difference between the primary side voltage ($V_{aa'}$) and the output voltage of the DC side converter ($V_{bb'}$). The current flowing through La is the integral of the voltage, and the power transferred through La is calculated by multiplying the voltage and current of La. Figure 2 indicates that the average power remains positive for both supply polarities.

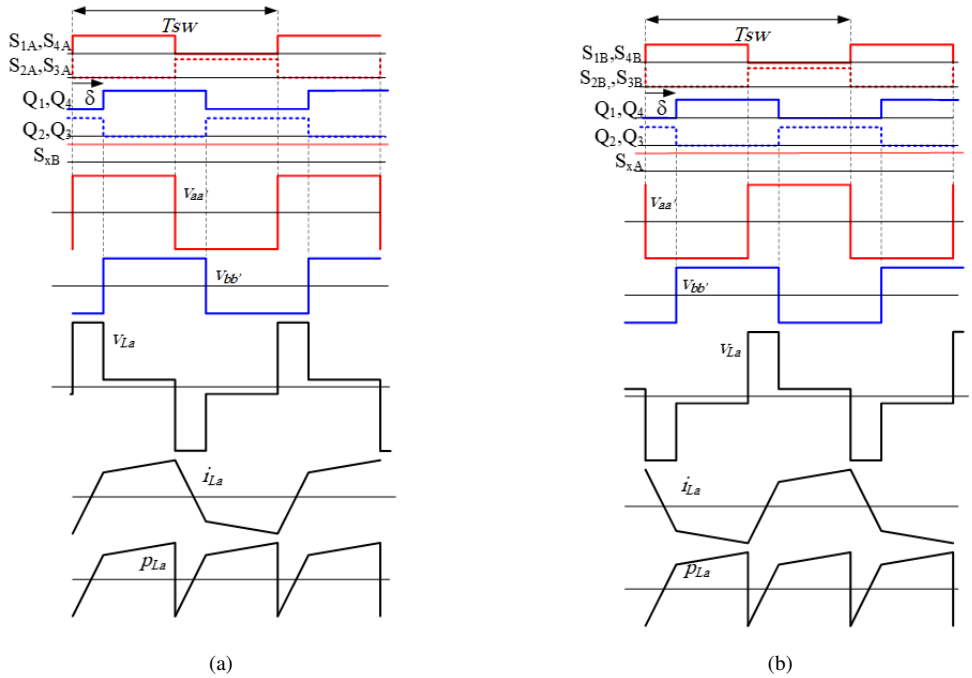

Figure 2. Switching signals, converters and La voltages, La current, and power flow when the converter functions to transfer energy from the AC side to the DC side: (a) V_{ac} positive; (b) V_{ac} negative

3 Current Equations and Basic Modulation Functions

The control variable that determines the power flow from the AC side to the DC side is the phase-shift angle (δ), which refers to the phase difference between the primary and secondary bridge voltage waveforms measured as the delay of the switching instant of the DC bridge with respect to the AC bridge. In practical applications, the variable δ can be modified by altering the phase-shift angle of the switching signals at one terminal of the transformer.

Assuming that the switching frequency is much higher than the AC line frequency, the AC line voltage is approximately constant during a switching cycle. The AC supply current during one switching cycle can be represented as $i_{ac,sw}$ [9]:

$$i_{ac,sw} = \frac{nV_{dc}}{L_a \pi \omega_{sw}} \delta(\pi - \delta) \tag{2}$$

where, $i_{ac,sw}$ during each commutation period is determined by δ. Therefore, the current waveform during a grid period can be controlled by changing δ during subsequent switching intervals, as defined by the modulation function. The current $i_{ac}(t)$ and the grid synthesized current $i_{ac,sw}$ in a grid period can be considered the same. Let $\frac{nV_{dc}}{La\pi\omega_{sw}} = 1$, Eq. (2) can be normalized and rewritten as follows:

$$i_{ac,sw} = \pi\delta(t) - \text{sign}(\delta(t)) * \delta(t)^2 \tag{3}$$

where, $\delta(t)$ represents a time-dependent function that characterizes the behavior of δ throughout a complete cycle of the AC supply. In addition, $(\delta(t))$ is +1 when $\delta(t)$ is positive and is -1 when $\delta(t)$ is negative. The sinusoidal and triangular functions are the basic modulation functions [10]. The following subsections describe these functions in the linear mode and introduce the suggested modification to operate in an overmodulation region.

In PWM converters, the modulation index regulates the voltage during each switching period by duty ratio adjustments. Overmodulation arises when the modulation index exceeds its maximum permissible limit. Consequently, the output of the converter reaches saturation at its peak value. In the overmodulation mode, the output voltage surpasses the maximum limit of the linear range, leading to a nonlinear output voltage variation and distorted output as the converter fails to accurately reproduce the reference signal. Overmodulation is considered to maximize output voltage at the expense of waveform quality.

In the present study, the concept of overmodulation was examined through two distinct methodologies. The initial approach involves the direct manifestation of the overmodulation concept by constraining the phase-shift angle to $\pi/2$ when the reference signal surpasses the peak value (1.0). The subsequent methodology aims to maintain the

overall reference signal below the maximum (1.0) while allowing the fundamental component of this signal to exceed 1.0 over an extended range by modifying the waveform through the incorporation of specific levels of harmonics within acceptable limits.

3.1 Sinusoidal Modulation Function

The sinusoidal modulation function shown in subgraph (a) of Figure 3 is given by:

$$\delta_{\sin}(t) = k\frac{\pi}{2}\sin(\omega_o t), (0 < k < 1) \tag{4}$$

where, $\delta_{\sin}$ is phase-shift angle, and k is the magnitude control ratio. The peak value of the delay that occurs at $\omega_o t = \pi/2$ is equivalent to a quarter of the switching cycle times k, where $k \leq 1$ in the linear mode. It can be observed that for the sinusoidal modulation function, the current waveform becomes more distorted at large values of k approaching 1 [16]. When applying the overmodulation concept in a straightforward manner, the sinusoidal modulation function in this mode saturates at $\delta = \pi/2$, as illustrated in subgraph (b) of Figure 3. Overmodulation $(k > 1)$ is achieved by applying a reference current that tends to produce a phase-shift angle greater than $\pi/2$. Since the maximum AC current value is attained at $\delta = \pi/2$, the modulation function is clipped at this level, as depicted in subgraph (b) of Figure 3.

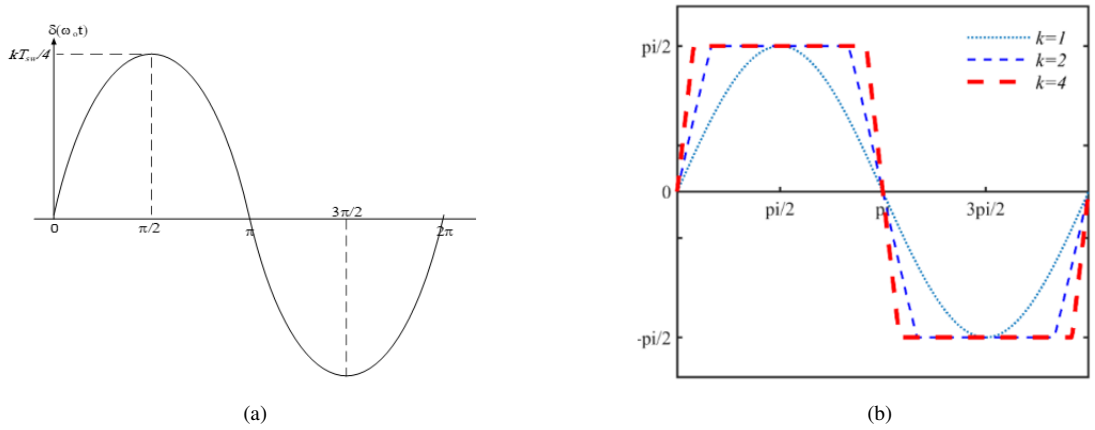

(a) (b)

Figure 3. Sinusoidal modulation function: (a) Linear mode; (b) Overmodulation mode

3.2 Triangular Modulation Function

The triangular modulation function is depicted in subgraph (a) of Figure 4. Throughout the supply voltage period, the phase shift changes linearly with the phase angle, reaching its peak at $\omega_o t = \pi/2$. In the linear region, the peak value of the delay is equal to $kT_{sw}/4$, where k is the magnitude control ratio $(-1 < k < +1)$. When k exceeds 1, allowing the converter to operate in the overmodulation mode, the modulation function in this scenario is clipped, as demonstrated in subgraph (b) of Figure 4.

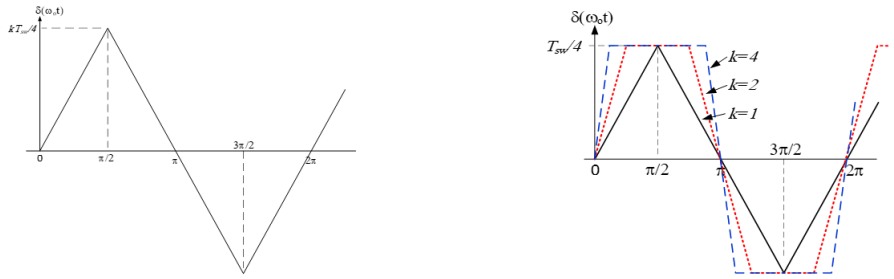

(a) (b)

Figure 4. Trigonometric modulation function: (a) Linear mode; (b) Overmodulation mode

4 BCMF

BCMF determines the phase-shift angle that results in a sinusoidal current waveform as a function of k and $\omega_o t$. This function is derived from the solution of Eq. (3) for a pure sinusoidal reference current, which is defined for unity power factor by Ahmed and AbdulKadir [16]:

$$i_{ac}(t)^* = kI_{\max,p} \sin(\omega_o t) \tag{5}$$

The resultant modulation function is given by:

$$\delta_{\text{mod}}\ (k, \omega_o t) = \frac{\pi - \sqrt{\pi^2 - 4kI_{\max,\,p} \sin(\omega_o t)}}{2} \tag{6}$$

$$I_{\max,p} = \frac{\pi}{4} \frac{nV_{dc}}{L_a \omega_{sw}} = \frac{nV_{dc}}{8L_a f_{sw}} \tag{7}$$

where, the current is the base current, represented by In=1.

4.1 Linear Mode

The angle δ was derived from Eq. (6) for a variety of k values and across the angular frequency range from 0 to 2π. The resulting BCMF is illustrated in subgraph (a) of Figure 5 for different k values. The modulation function displays diverse patterns contingent upon the value of k; nevertheless, the associated current waveform consistently maintains a sinusoidal form, as represented in subgraph (b) of Figure 5.

It is evident that determining the phase-shift angle for BCMF entails more intricate calculations in comparison to sinusoidal and triangular functions. However, with the availability of contemporary digital controllers operating at frequencies in the hundreds of megahertz range, the computation of delta from Eq. (6) can be accomplished in mere microseconds at most, which does not impede real-time implementation.

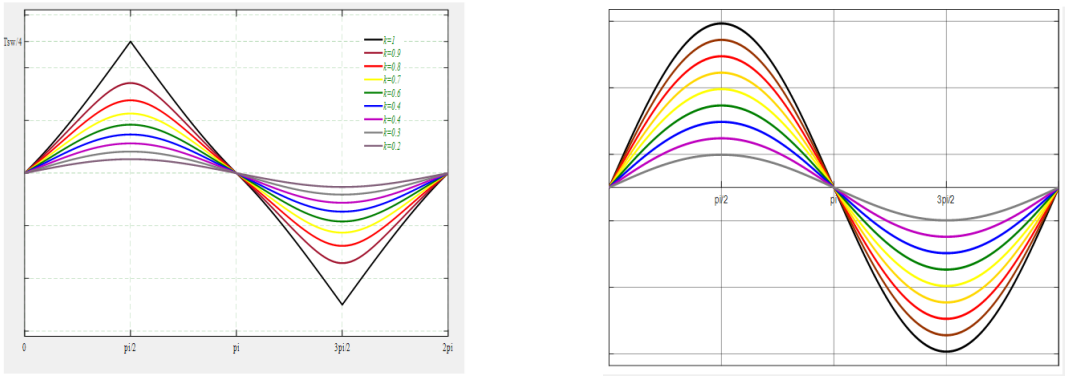

(a) (b)

Figure 5. BCMF and resultant current at different values of magnitude control ratio k: (a) BCMF; (b) AC current in BCMF

4.2 Overmodulation

The overmodulation region allows the converter to operate beyond the linear modulation range, providing higher output current. This study introduces an alternative approach by incorporating specific precalculated harmonics that enable the fundamental component to extend beyond the maximum value (attained at k = 1), while ensuring that the overall reference signal remains within the bounds of linear modulation (maximum $\leq$ 1).

Eq. (7) outlines the highest allowable peak current that the converter can output in the linear mode. The recommended strategy for overmodulation concentrates on creating a reference current with several characteristics: (i) the reference current signal includes a fundamental component together with a restricted set of higher odd harmonics; (ii) it keeps the peak reference current under the maximum current level described in Eq. (7); (iii) the amplitude of the fundamental component in the reference current exceeds the maximum limit indicated by Eq. (7); and (iv) the amount of higher-order harmonics is limited by the current distortion standard.

Figure 6 illustrates the proposed approach for k = 1.12, signifying a reference current extended by 12% beyond the linear modulation range limit. It can be observed that the fundamental component surpasses the highest control range. To bring the total current back within the controllable range, five harmonic components were introduced, as depicted in Figure 6.

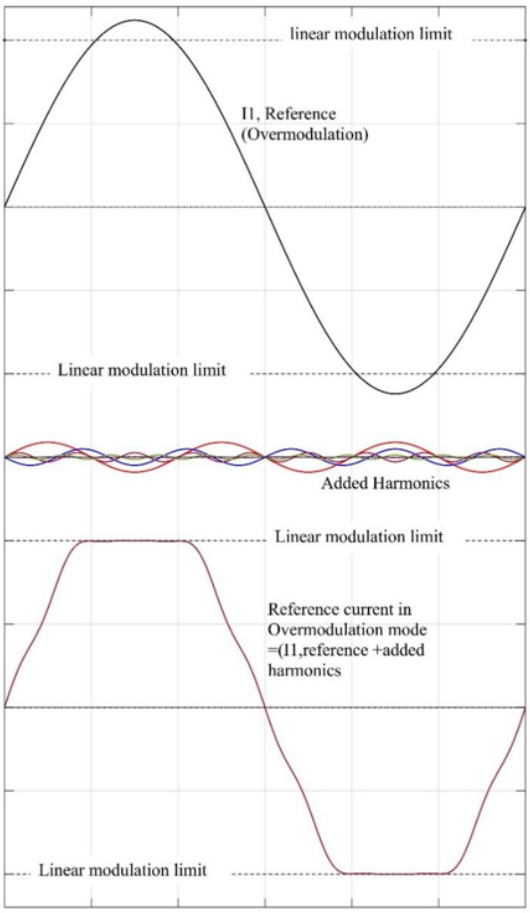

Figure 6. Reference current waveform for the overmodulation function (k = 1.12)

The amplitudes of different harmonics need to be computed for each reference fundamental within the feasible range. These calculations were performed offline using the Matlab optimization function "fmincon." The amplitudes of different harmonics (A3, A5, etc.) were constrained in accordance with the IEEE Std 519 standard issued by the Institute of Electrical and Electronics Engineers (IEEE), as shown in Table 2 [11]. The minimization function was resolved for the lowest ID representing the short circuit current level (commencing from A1, as indicated in Table 2). If the minimization criterion is not met, an attempt is made with the harmonics tolerance corresponding to the subsequent ID. The outcome of the minimization function is illustrated in Figure 7.

Table 2. Key parameters of the proposed model distortion (%) of load demand current adopted from the IEEE Std 519

ID	ISC	Harmonic Order (odd harmonics)				
		< 11	$11 < h < 17$	$17 < h < 23$	$23 < h < 35$	$35 < h$
$A1$	$< 20^*$	4	2	1.5	0.6	0.3
$A2$	$20 < 50$	7	3.5	2.5	1	0.5
$A3$	$50 < 100$	10	4.5	4	1.5	0.7
$A4$	$100 < 1000$	12	5.5	5	2	1
$A5$	> 1000	15	7	6	2.5	1.4

Note: Maximum harmonic current distortion (%) of load demand current (0.12-69 KV) based on Table 2, IEEE Std 519-1992

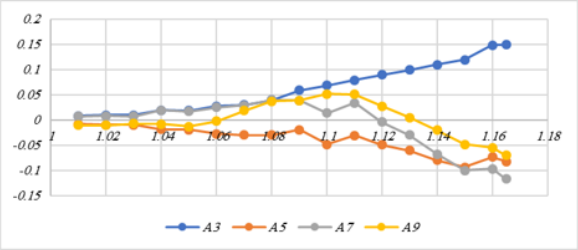

Figure 7. Solution of the optimization function over the feasible range of A1

Following the IEEE Std 519 is essential for controlling harmonics in power systems, ensuring quality and compliance. This compliance limits THD and individual harmonic distortion (IHD) to avoid high harmonic currents. This results in improved reliability and prevents damage, as excessive harmonics can cause overheating and efficiency loss in transformers, motors, and capacitors. Complying with the IEEE Std 519 is important for power quality, preventing equipment damage, and meeting utility standards. It lowers operational risks, boosts system efficiency, and enhances stability in contemporary power grids.

5 Simulation and Results

TThe bidirectional AC-DC converter system was assessed through SIMULINK modelling, utilizing the parameters outlined in Table 3.

Table 3. The paremeters of the bidirection AC-DC converter system

Part	Parameters
AC supply	$220\ \mathrm{V}, 50\ \mathrm{Hz}$
AC filter	$\mathrm{Lf} = 70\mu\mathrm{H}, \mathrm{rL} = 0.4\Omega, \mathrm{Cf} = 132\mathrm{uF}, \mathrm{rC} = 10\ \mathrm{m}\Omega$
Ron (Mosfet)	0.1Ω
Rd (Mosfet)	0.01Ω
R Snubber (Mosfet)	$100\mathrm{k}\Omega$
Tranformer	$n = 1, 5\mathrm{kVA}, \mathrm{Fsw} = 10\mathrm{kHz}$
Series Inductor	$\mathrm{La} = 0.15\mathrm{mH}$ with $\mathrm{ESR} = 0.1\Omega$
DC side converter	The mosfet parameters: Roff = 1e5, Ron=1e-3
DC supply	350 V

5.1 Converter Operation in the Linear Range

The converter controlled in the linear mode with three modulation functions (sinusoidal, triangluar and BCMF) was simulated for values of the magnitude control ratio (k): 1 and 0.6. The waveforms of the resulting $i_{ac}(t)$ and the instantaneous current are shown in Figure 8. The sinusoidal modulation function experiences significant distortion when k = 1. For lower k, THD decreases. The triangular modulation function operates with minimum distortion when k = 1. As k decreases, the current becomes more distorted. The current waveforms corresponding to BCMF have the least distortion.

5.2 Converter Operation in the Overmodulation Region

The formation of the basic reference functions in the overmodulation region is illustrated in subgraph (b) of Figure 3 and subgraph (b) of Figure 4 for the sinusoidal and triangular modulation functions, respectively. The additional power achieved in the overmodulation mode is 10% and 24% for sinusoidal and triangular modes, respectively. However, operating in overmodulation leads to a considerable increase in harmonic distortion.

In the case of BCMF, the inclusion of odd harmonics maintains the peak value of the normalized reference current below 1, allowing k to range between $1 < k < 1.165$. This extension of the linear relationship between k and the transferred power is demonstrated to be 16.5% beyond the linear control level, as depicted in Figure 9. Beyond this limit, the optimization function ”fmincon” no longer satisfies the minimization condition, resulting in the total amplitude of the normalized reference function exceeding 1 and becoming limited by clipping. At this point, the overmodulation performance of BCMF becomes comparable to that of other modulation functions.

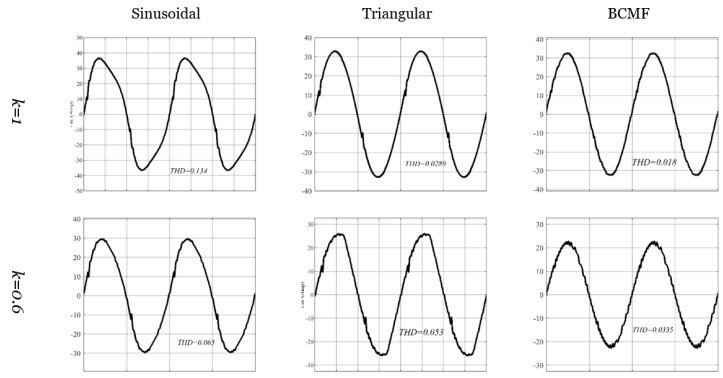

Figure 8. Current waveforms of the three modulation functions in the linear range ($k < 1$)

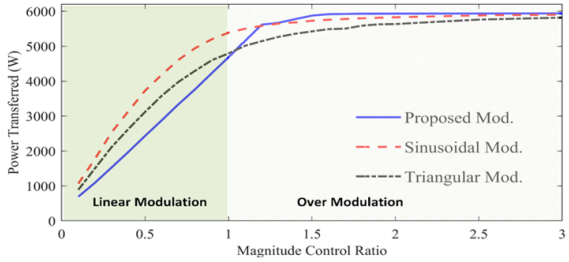

Figure 9. Relation between power transferred and magnitude control ratio (k)

Figure 10 reveals that the proposed BCMF yields the minimum harmonic distortion in both linear and overmodulation regions for a given power transfer value. This approach is shown to adhere to the IEEE Std 519 for IDs A1 and A2 across wider ranges compared to other modulation functions.

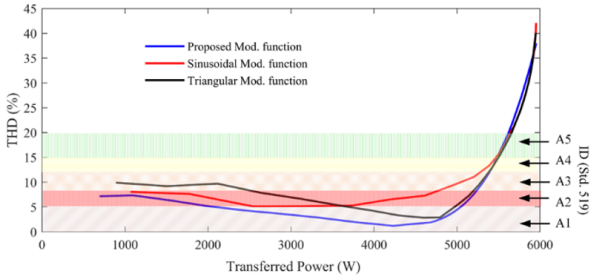

Figure 10. Relation between THD and the transferred power

Table 4 presents a comparison of the proposed approach against the features of various DAB PSM strategies found in the existing literature. The latest research in this area primarily aims to minimize harmonic distortion, broaden the ZVS range, and enhance performance by incorporating a variable switching frequency. This research intends to offer an expanded power transfer range to leverage the occasional peak power available in PV systems at peak time. This presented method operates under constant switching frequency, thereby preventing a reduction in the permeability of the magnetic materials and mitigating the control task.

6 Conclusion

This study investigates a single-phase, single-stage, bidirectional AC-DC power converter designed for use in electric micro-grids. The AC bridge comprises four bidirectional switching modules. Through the analysis of the PSM control, the influence of different modulation methods on AC current waveforms was examined using two basic modulation functions: sinusoidal and triangular. It is evident that the sinusoidal modulation function introduces notable current distortion when the magnitude control ratio (k) is near 1, while the triangular modulation function exhibits high distortion for small k values. This research considers BCMF, which offers linear control and minimal harmonic distortion across all k values.

Table 4. Comparison of the proposed BCMF with other recent DAB PSM strategies

Modulation Technique	Main Advantages	Limitations	Reference
Single Phase Shift (SPS)	Simple implementation and widely used	Higher power loss and narrower ZVS range	[17]
EPS	Wider ZVS range and reduced backflow power	More complex control logic	[18]
Dual Phase Shift (DPS)	Improved power transfer and wider operating range	More complex control strategy	[19]
Triple Phase Shift (TPS)	Minimizes peak current stress and increases efficiency	Increased complexity in control	[20]
Proposed BCMF	Constant switching frequency and extended linear power control range	Higher switching losses and limited ZVS	

This study focuses on operation in the overmodulation region, with the aim of extending power transfer capabilities while keeping other circuit parameters fixed. An innovative approach was introduced specifically for BCMF, expanding the linear-like operational characteristics by approximately 16%. This approach involves incorporating a limited amount of odd harmonics to ensure the total reference current signal remains within achievable limits. Optimization calculations were employed to determine the necessary amplitudes of harmonics to be added for different reference values. A simulation study was conducted to assess the performance of the three modulation methods in both linear and overmodulation modes. Within the overmodulation region, the proposed BCMF shows superior performance in terms of linearity and harmonic distortion.

While numerous recent studies in this area seek to broaden the ZVS region to reduce switching losses by incorporating trapezoidal and triangular operation modes, this study has not considered this alternative and instead concentrates on the square wave switching mode, which ensures maximum power transfer. This approach results in a minimal ZVS region, consequently leading to an expectation of reduced operational efficiency.

Data Availability

The data used to support the research findings are available from the corresponding author upon request.

Conflicts of Interest

The authors declare no conflict of interest.

References

[1] B. Meng, R. C. Loonen, and J. L. Hensen, "Data-driven inference of unknown tilt and azimuth of distributed pv systems," *Sol. Energy*, vol. 211, pp. 418–432, 2020. https://doi.org/10.1016/j.solener.2020.09.077

[2] Q. Hassan, M. K. Abbas, A. M. Abdulateef, J. Abdulateef, and A. Mohamad, "Assessment the potential solar energy with the models for optimum tilt angles of maximum solar irradiance for Iraq," *Case Stud. Chem. Environ. Eng.*, vol. 4, p. 100140, 2021. https://doi.org/10.1016/j.cscee.2021.100140

[3] E. E. Henao-Bravo, C. A. Ramos-Paja, and A. J. Saavedra-Montes, "Adaptive control of photovoltaic systems based on dual active bridge converters," *Computation*, vol. 10, no. 6, p. 89, 2022. https://doi.org/10.3390/computation10060089

[4] J. Zhang, D. Sha, and M. Peisong, "A dual active bridge DC–DC-based single stage AC–DC converter with seamless mode transition and high power factor," *IEEE Trans. Ind. Electron.*, vol. 69, no. 2, pp. 1411–1421, 2022. https://doi.org/10.1109/TIE.2021.3057016

[5] A. Mishra and M. Singh, "A 10-kw active front end rectifier fed dual active bridge converter for ev charging," in *2023 4th International Conference for Emerging Technology (INCET)*, Belgaum, India, 2023, pp. 1–6. https://doi.org/10.1109/INCET57972.2023.10170584

[6] M. Gierczynski, L. M. Grzesiak, and A. Kaszewski, "A dual rising edge shift algorithm for eliminating the transient dc-bias current in transformer for a dual active bridge converter," *Energies*, vol. 14, no. 14, p. 4264, 2021. https://doi.org/10.3390/en14144264

[7] R. Baranwal, G. F. Castelino, K. Iyer, K. Basu, and N. Mohan, "A dual-active-bridge-based single-phase ac to dc power electronic transformer with advanced features," *IEEE Trans. Power Electron.*, vol. 33, no. 1, pp. 313–331, 2018. https://doi.org/10.1109/TPEL.2017.2669148

[8] T. Chen, R. Yu, Q. Huang, and A. Q. Huang, "A single-stage bidirectional dual-active-bridge ac-dc converter based on enhancement mode gan power transistor," in *2018 IEEE Applied Power Electronics Conference and Exposition (APEC)*, San Antonio, TX, USA, 2018, pp. 723–728. https://doi.org/10.1109/APEC.2018.8341092

[9] M. Llomplat, J. E. Bosso, R. E. Carballo, and G. O. García, "Novel modified phase-shift modulation strategy for isolated ac–dc power converters," *IET Power Electron.*, vol. 13, no. 5, pp. 965–975, 2020. https://doi.org/10.1049/iet-pel.2019.0895

[10] B. Zhao, Q. Song, and W. Liu, "Power characterization of isolated bidirectional dual-active-bridge dc–dc converter with dual-phase-shift control," *IEEE Trans. Power Electron.*, vol. 27, no. 9, pp. 4172–4176, 2012. https://doi.org/10.1109/TPEL.2012.2189586

[11] H. Zhou and A. M. Khambadkone, "Hybrid modulation for dual active bridge bi-directional converter with extended power range for ultracapacitor application," in *2008 IEEE Industry Applications Society Annual Meeting*, Edmonton, AB, Canada, 2008, pp. 1–8. https://doi.org/10.1109/08IAS.2008.275

[12] K. Yamanokuchi, H. Watanabe, and J. Itoh, "Three-phase DAB type AC-DC converter using 9-switch matrix converter," *IEEJ Trans. Ind. Appl.*, vol. 144, no. 2, pp. 37–46, 2024. https://doi.org/10.1541/ieejias.144.37

[13] X. X. Chen, J. W. Liu, K. H. Loo, D. Mou, and Q. C. Song, "Steady-state modeling of a matrix-type ac-dc dab converter considering ac-side capacitor voltage ripple," in *2024 CPSS & IEEE International Symposium on Energy Storage and Conversion (ISESC)*, Xi'an, China, 2024, pp. 114–119. https://doi.org/10.1109/ISESC63657.2024.10785390

[14] D. Guo, P. Wang, C. Ren, and J. M. Guerrero, "Variable frequency phase-shift modulation technique for single stage dual-active-bridge ac-dc converter," in *2023 11th International Conference on Power Electronics and ECCE Asia (ICPE 2023 - ECCE Asia)*, Jeju Island, South Korea, 2023, pp. 524–529. https://doi.org/10.23919/ICPE2023-ECCEAsia54778.2023.10213554

[15] S. Komeda, S. Takuma, and Y. Ohnuma, "Variable switching frequency control for a dual-active-bridge single-phase ac-dc converter with active energy buffer," *IEEJ J. Ind. Appl.*, vol. 12, no. 3, pp. 418–426, 2023. https://doi.org/10.1541/ieejjia.22007817

[16] M. F. Ahmed and M. N. Abdul Kadir, "Phase shift modulation strategy for single stage ac to dc dual active bridge converter," *Iraqi J. Electr. Electron. Eng.*, vol. 20, no. 1, p. 17, 2024. https://doi.org/10.37917/ijeee.20.1.17

[17] G. A. Mudiyanselage, N. Keshmiri, and A. Emadi, "Comparative analysis of single phase shift control and optimized extended phase shift control of dual active bridge converters for wide voltage range applications," in *IECON 2023- 49th Annual Conference of the IEEE Industrial Electronics Society (IECON)*, Singapore, 2023, pp. 1–6. https://doi.org/10.1109/IECON51785.2023.10312217

[18] V. Tiwari, M. Asim, M. T. Alam, M. I. Siddiqui, and M. Alam, "Implementation of single-phase shift (SPS) and extended phase shift (EPS) for dual active bridge (DAB)," *Indian J. Sci. Technol.*, vol. 17, no. 41, pp. 4262–4269, 2024. https://doi.org/10.17485/ijst/v17i41.2456

[19] M. J. Baig and R. K. Singh, "Dual active bridge converter's inherent soft switching steady-state analysis with single and dual phase shift modulation," in *2024 IEEE International Students' Conference on Electrical, Electronics and Computer Science (SCEECS)*, Bhopal, India, 2024, pp. 1–5. https://doi.org/10.1109/SCEECS61402.2024.10481953

[20] S. Tiwari and S. Sarangi, "Comparison of current stress for different modulation techniques in dual active bridge converter," in *2019 International Conference on Electrical, Electronics and Computer Engineering (UPCON)*, Prayagraj, India, 2019. https://doi.org/10.1109/UPCON47278.2019.8980050